Available online at www.sciencedirect.com
ScienceDirect
Trans. Nonferrous Met. Soc. China 29(2019) 1200−1210
Transactions of Nonferrous Metals Society of China
www.tnmsc.cn

Anodizing parameters for superheated slurry cast 7075 aluminum alloys

Itsaree IEWKITTHAYAKORN[1], Somjai JANUDOM[1,2],
Narissara MAHATHANINWONG[2,3], Seppo KARRILA[3], Jessada WANNASIN [1,2]

1. Department of Mining and Materials Engineering,
Faculty of Engineering, Prince of Songkla University, Hat Yai, Songkhla 90112, Thailand;
2. Center of Excellence in Materials Engineering (CEME),
Faculty of Engineering, Prince of Songkla University, Hat Yai, Songkhla 90112, Thailand;
3. Faculty of Science and Industrial Technology,
Prince of Songkla University, Surat Thani Campus, Surat Thani 84000, Thailand

Received 19 August 2018; accepted 28 December 2018

Abstract: The anodizing parameters of voltage, current density, temperature, and electrolyte choice were assessed to find an appropriate combination for the superheated slurry cast 7075 Al alloy substrate. The alloy was anodized in sulfuric acid electrolyte or alternatively in sulfuric acid mixed with boric acid or citric acid. The voltages applied were in the range of 15−30 V. Anodizing current densities tested were 2 and 3 A/dm^2, while temperatures tested were 5 and 15 °C. Thickness, surface morphology, hardness, and corrosion resistance of the oxide film were then evaluated. It was found that 25 V, 2 A/dm^2 and 5 °C were suitable for this alloy when anodized in sulfuric acid. The oxide film was smooth with uniform thickness, low porosity, high hardness, and had the highest corrosion resistance at these parameters. However, discontinuous oxide films were observed from samples anodized at higher temperature of 15 °C. Alternative electrolytes considered were sulfuric acid mixed with boric acid or citric acid. The results showed that electrolytes with boric acid or citric acid increased thickness, hardness, corrosion resistance and quality of the oxide films. However, these oxide films were inferior to those obtained with sulfuric acid electrolyte at lower temperature (25 V, 2 A/dm^2 and 5 °C).

Key words: 7075 aluminum alloy; superheated slurry casting; anodization; oxide film; anodizing parameters

1 Introduction

The 7075 aluminum alloy is lightweight and has high strength and good corrosion resistance. This alloy is widely used in aircrafts, sports, and various engineering applications. The high strength 7075 aluminum alloy is generally produced by a wrought process, which has many steps and incurs high production costs. Alternative cast production processes for the 7075 aluminum alloy have been widely explored [1−4], and the gas induced semi-solid (GISS) process has been proposed by WANNASIN et al [1]. Studies on GISS 7075 aluminum alloy have been continually pursued for the past eight years. These studies have covered the forming process [1,5], the heat treatment [6−8], property tests [7,9,10], and applications [11]. The GISS process is a superheated slurry casting process. Superheated slurry cast 7075 aluminum alloys need anodization for the corrosion protection [12] and this aspect is experimentally assessed in this work.

The anodization of aluminum is an electrochemical process, forming anodized aluminum oxide (AAO), so that the oxide film covers and shields the surface of the aluminum substrate. Anodizing requires appropriate choices of electrolyte, voltage, current density, temperature, and duration of treatment [13]. Sulfuric acid has been widely used as the anodizing electrolyte [14] because it has lower cost and gives better anodic films than oxalic, chromic, or phosphoric acids. Studies have also addressed on the mixed electrolytes, such as sulfuric−oxalic acid [15], sulfuric−nitric acid, and sulfuric−boric acid [14]. The anodizing voltage is known to affect the thickness of the oxide film [16]. THEOHARI and KONTOGEORGOU [17] reported that the thickness of the oxide film on pure Al and 5052 Al alloy increases as the anodizing temperature is increased in the range of 10−30 °C, and then decreases at

Corresponding author: Somjai JANUDOM; Tel: +66-945-842-504; E-mail: somjai.ja@psu.ac.th
DOI: 10.1016/S1003-6326(19)65027-2

temperatures beyond 40 °C. In addition, increasing the current density increases the growth rate of oxide film [18]. On the other hand, Al−Fe and Al−Fe−Si particles in binary and ternary aluminum substrates are occluded in the oxide film next to Si particles, blocking locally the oxide growth, whereas Al_2Cu particles are preferentially oxidized [19]. Deflected pores are also found around the Si particles.

The anodization of 7075 Al alloy was investigated, and intermetallic particles commonly formed in the microstructure negatively impacted the quality of oxide film [20]. Low contents (below 0.1 wt.%) of Si and Fe elements in the 7075 Al alloy give better anodization response [21,22]. In addition, the 7075 Al alloy has high contents of Zn, Mg, and Cu alloying elements, and these tend to form $MgZn_2$ and Al_2Cu intermetallic particles after casting. The superheated slurry cast 7075 aluminum alloy still has these intermetallic particles in the microstructure, while low rate of defects and low production costs are the main advantages. Anodizing this alloy requires knowledge of suitable anodizing parameters. Therefore, this work aimed to determine suitable anodizing parameters for the superheated slurry cast 7075 aluminum alloy.

2 Experimental

2.1 Materials and anodizing process

The superheated slurry cast 7075 Al alloy was produced by squeeze casting. The alloy ingots were molten at 750 °C, and then the semi-solid slurry was injected with nitrogen gas for 3 s at 645 °C into a square-shaped mold (100 mm × 100 mm × 15 mm). The squeeze casting was done at a pressure of approximately 80 MPa. The chemical composition of the alloy was Al−6Zn−2.7Mg−1.73Cu−0.14Fe−0.06Si. The cast plates were cut to specimens (30 mm × 30 mm × 8 mm) that were heat-treated at 450 °C for 4 h, followed by quenching in water at room temperature, and then artificial aging at 145 °C for 6 h [7]. All the samples were firstly abraded with sand papers (320 to 1200 grid) and then polished with 5 and 1 μm alumina powders for surface finish.

For anodizing, the specimens were degreased in Aluclean 25 solution (50 g/L) at 60 °C for about 5 min, rinsed with water, subsequently etched in NaOH solution (100 g/L) at 55 °C for about 1 min, and then rinsed with water. The specimens were then desmutted in HNO_3 solution (200 mL/L) at room temperature for about 2 min, and rinsed with water and dried: this removed the black layer formed on the surface. The anodizing electrolyte, voltage, current density, and temperature that were experimentally tested in this work are summarized in Table 1. Temperature control of the solutions was achieved by using a bath chiller with temperature controller and K-type thermocouple as the sensor. In addition, the voltage and current were adjustable by using a switching DC power supply (SPS−3610, GW Instek, Taiwan, China). After the circuit was closed, the power supply automatically transitioned from constant voltage (CV) to constant current (CC) control mode. The current per total surface area of specimen was determined and reported as the current density.

Table 1 Experimental anodizing parameters

Sample No.	Electrolyte	Current density/(A·dm^{-2})	Voltage/V	Temperature/°C	Time/min
H1-2-15-15	H_2SO_4 (55 mL/L)	2	15	15	60
H1-2-20-15	H_2SO_4 (55 mL/L)	2	20	15	60
H1-2-25-15	H_2SO_4 (55 mL/L)	2	25	15	60
H1-2-30-15	H_2SO_4 (55 mL/L)	2	30	15	60
H1-3-15-15	H_2SO_4 (55 mL/L)	3	15	15	60
H1-3-20-15	H_2SO_4 (55 mL/L)	3	20	15	60
H1-3-25-15	H_2SO_4 (55 mL/L)	3	25	15	60
H1-3-30-15	H_2SO_4 (55 mL/L)	3	30	15	60
H1-2-20-5	H_2SO_4 (55 mL/L)	2	20	5	60
H1-2-25-5	H_2SO_4 (55 mL/L)	2	25	5	60
H1-B1-2-25-15	H_2SO_4 (55 mL)+H_3BO_3(30.92 g/L)	2	25	15	60
H1-B2-2-25-15	H_2SO_4 (55 mL)+ H_3BO_3 (61.83 g/L)	2	25	15	60
H2-B2-2-25-15	H_2SO_4 (109 mL)+ H_3BO_3 (61.83 g/L)	2	25	15	60
H1-CH1-2-25-15	H_2SO_4 (55 mL)+$C_6H_8O_7$ (153.40 g/L)	2	25	15	60
H2-CH2-2-25-15	H_2SO_4 (109 mL)+$C_6H_8O_7$ (315.21 g/L)	2	25	15	60

After anodizing, the samples were rinsed with water. Finally, the specimens were immersed in dye color at room temperature for about 15 min, transferred for sealing into hot water with Aluseal 20 solution (4 g/L) at 95−100 °C for 10 min, and dried.

2.2 Property tests and microstructure observation

2.2.1 Film thickness and color

The average film thickness of the anodic oxide layer was measured by optical microscopy (Axio Scope.Al, ZEISS, Germany) combined with image analysis, and the calculations were as described in Ref. [23]. For film thickness measurement, the anodized alloys were longitudinally cut to 5 mm × 30 mm × 8 mm size with a low speed diamond saw (Miniotom, Struers) and then spray painted with white color. Subsequently, the anodized alloys were hot mounted, ground with SiC sand paper (grid P320−P1200), and polished with suspended alumina powders (5 and 1 μm).

The surface color was measured with an HP−200 precise color reader (China) [24]. Measurements were taken at three positions on the diagonal surface for each anodized alloy.

2.2.2 Vickers microhardness

The hardness of coating was measured by a digital microhardness tester (Matsuzawa MMT-X7, Japan). All measurements used 25 g load for 15 s [25]. The average hardness of anodic film was obtained from nine measured points on flat surfaces of each sample.

2.2.3 Corrosion tests

The corrosion tests of un-anodized and anodized alloys H1-2-15-15, H1-2-25-15, H1-2-25-5, H2-B2-2-25-15, and H2-CH2-2-25-15 followed ASTM G 31-72 (2004), which used 42 g of NaCl in 1500 mL of water at 40−45°C. The pH was from 6.0 to 7.0 in test tubes used to expose the samples for 336 h, and the mass loss to nearest milligram was recorded. The corrosion rates were expressed in millimeters per year (mm/a) [26,27].

2.2.4 Microstructure examination

The microstructure of anodic surface film was imaged by optical microscopy (OM: Axio Scope.Al, ZEISS, Germany) and by scanning electron microscopy (SEM: FEI, Quanta 400). The sample preparation was described in Section 2.2.1.

The surface porosities on the anodized alloys H1-2-15-15, H1-2-25-15, H1-2-25-5, H2-B2-2-25-15, and H2-CH2-2-25-15 were examined by field emission scanning electron microscopy (FE-SEM: Merlin compact, Zeiss, Germany) and by energy dispersive X-ray spectrometer (Oxford, Aztec). Analysis of the FE-SEM images for the surface porosity was performed with ImageJ software, estimating the area fraction on the total oxide coating that was occupied by nanopores [28].

3 Results and discussion

3.1 Microstructure of superheated slurry cast 7075 Al alloy substrate

The microstructure of superheated slurry cast 7075 Al alloy had non-dendritic grains and two main phases: α-Al phase and grain boundary (GB) of the eutectic mix of (α-Al+η-$MgZn_2$), $Al_2Mg_3Zn_3$, Al_2CuMg, Mg_2Si; and Fe-rich phase [6,12,21,22]. Figure 1(a) shows secondary phase particles in the microstructure of the alloy after T6 heat treatment. Two colors at the grain boundaries are clearly seen in Fig. 1(b). The white phase is composed of Zn, Cu and Fe, while the coarse black phase is composed of Mg and Si, according to the EDS point analysis in Figs. 1(c) and (d). MAHATHANINWONG et al [7] reported that the secondary phase found in cast slurry semi-solid 7075 Al alloy consists of Al_7Cu_2Fe, Al_6Fe and Mg_2Si. Because Zn in the Al (Cu, Fe, Zn) particles can easily diffuse to the α-Al matrix, Mg and segregated sluggish silicon are left behind to form coarse black Mg_2Si particles. These secondary particles can either contribute to or obstruct the growth of the oxide film on 7075 Al alloy substrate, depending on particle type and size [19,20,22].

3.2 Characterization of oxide film on superheated slurry cast 7075 Al alloy substrate anodized in sulfuric acid electrolyte

Figure 2 shows cross-section micrographs of the oxide films on 7075 Al alloy substrates after anodizing in sulfuric acid (55 mL/L) electrolyte at various voltages, current densities, and temperatures. It can be observed that the thickness of oxide film (Table 2) increased with voltage from 15 to 30 V (at 2 A/dm^2, 15 °C, 60 min), as shown in Figs. 2(a−d). The average oxide film thickness (Table 2) obtained at 15 V was very thin, 2.78 μm, and increased to 14.59 μm at 25 V. MUBAROK et al [16] proposed that increased voltage leads to higher O^{2-} and Al^{3+} mobilities that increase the oxide film thickness. The oxide film thicknesses at 25 and 30 V did not differ obviously, indicating that 25 V is optimal for anodizing in sulfuric acid electrolyte, giving the thickest oxide film. However, the oxide films obtained were non-uniform and the substrate/oxide interfaces were disturbed by secondary particles. Representative SEM images of such flaws are shown in Fig. 3. It can be also seen that secondary Mg−Si particles were embedded in the oxide films. They gradually reduced to form Si-containing particles, and an example was shown by the arrow in Fig. 3(a). Cavities were also formed near the remaining Si particles, as indicated by the arrow in Fig. 3(b) and confirmed by the EDS results in Fig. 3(c). The current density was locally increased nearby these particles,

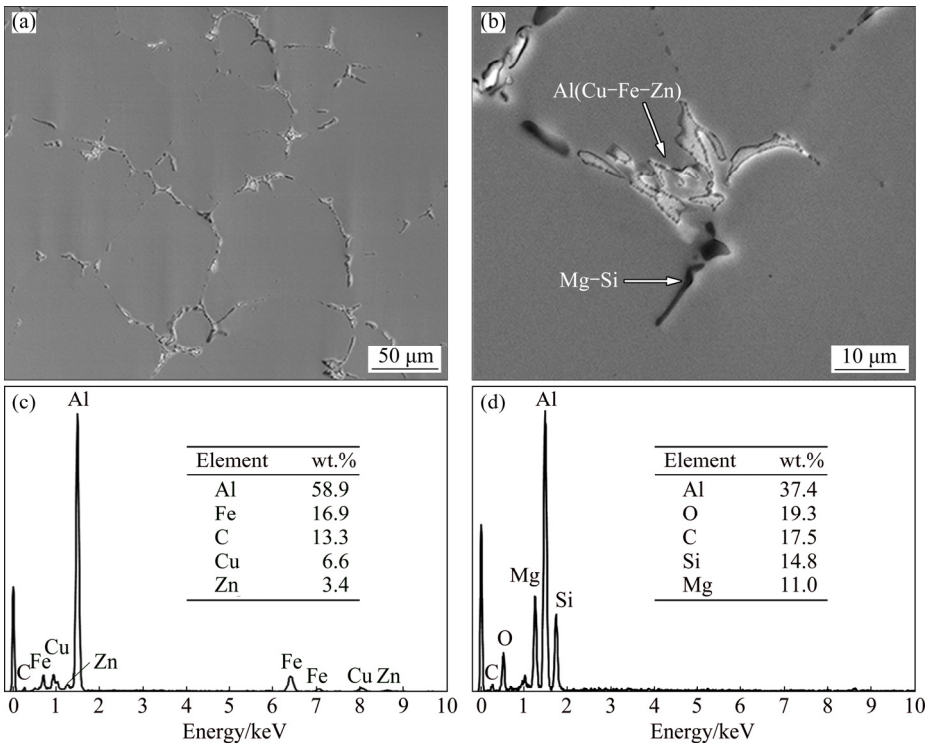

Fig. 1 SEM images of second phase particles in microstructure of alloy after T6 heat treatment (a, b), and EDS analysis of gray phase (c) and coarse black phase (d)

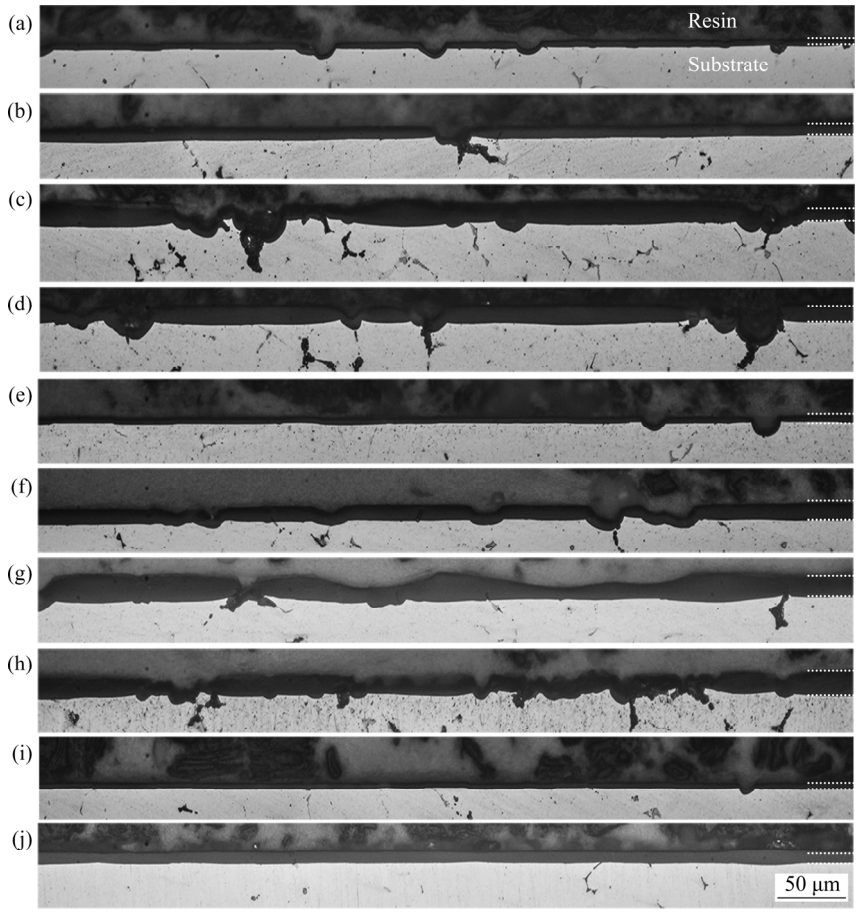

Fig. 2 Cross-section micrographs of oxide films on different anodized samples (white dashed lines show oxide film boundaries): (a) H1-2-15-15; (b) H1-2-20-15; (c) H1-2-25-15; (d) H1-2-30-15; (e) H1-3-15-15; (f) H1-3-20-15; (g) H1-3-25-15; (h) H1-3-30-15; (i) H1-2-20-5; (j) H1-2-25-5

Table 2 Film thickness and other properties of anodic oxide layer on as-cast 7075 Al alloy

Sample No.	AAO film thickness/μm	Hardness of AAO film (HV)	Lightness, *L*	Yellowness, *b*
H1-2-15-15	2.78±0.83	248.33±13.18	83.37±0.43	41.86±1.19
H1-2-20-15	7.41±0.88	234.87±6.29	81.42±0.15	57.77±1.82
H1-2-25-15	14.59±0.98	185.07±15.28	75.08±0.55	66.69±0.62
H1-2-30-15	15.81±1.61	171.16±10.92	75.60±0.48	66.48±2.37
H1-3-15-15	4.07±1.21	252.22±11.09	84.50±0.45	32.86±1.81
H1-3-20-15	10.00±1.44	237.23±12.81	78.62±0.66	66.25±0.26
H1-3-25-15	15.93±1.21	146.82±25.18	75.17±0.06	68.11±0.50
H1-3-30-15	17.25±1.20	125.26±20.05	75.67±0.23	68.07±1.07
H1-2-20-5	3.33±0.00	239.66±10.01	84.40±0.23	43.46±0.96
H1-2-25-5	9.07±1.21	315.28±11.48	79.39±0.27	71.54±0.43
H1-B1-2-25-15	16.85±1.30	210.32±39.79	77.38±0.51	73.84±0.61
H1-B2-2-25-15	19.26±0.88	254.24±21.45	77.54±0.80	74.07±1.24
H2-B2-2-25-15	22.78±1.18	265.12±11.3	76.50±0.25	74.46±0.83
H1-CH1-2-25-15	16.48±1.00	292.67±44.07	78.41±0.06	66.82±1.16
H2-CH2-2-25-15	24.81±1.30	347.04±40.34	68.33±0.15	57.36±0.45

Color coordinate *L* is 100 for lightest and 0 for darkest, while *b* indicates yellow by positive values and blue by negative values

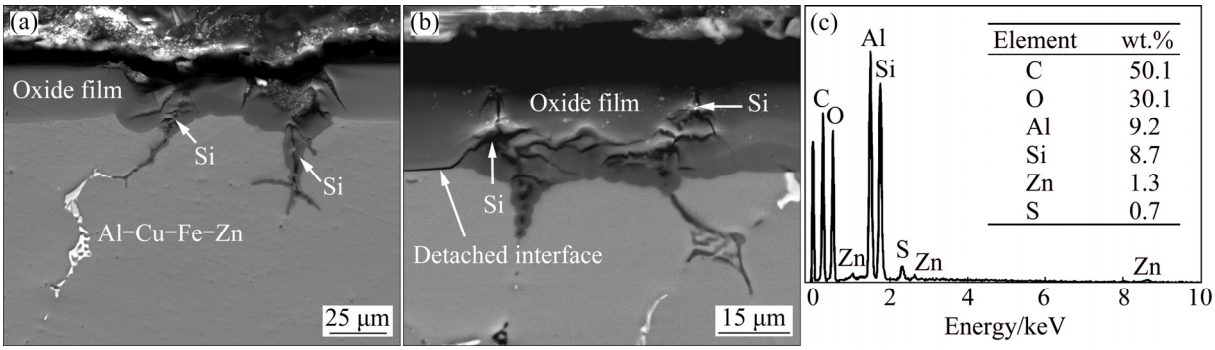

Fig. 3 SEM imges (a, b) and EDS analysis (c) of secondary phase particles embedded in anodic oxide films

which accelerated the ionization of the neighboring Al matrix to form a concave interface [29]. On the other hand, it has been reported that secondary particles of Al_3Fe, Al_7Cu_2Fe, and Al_2Cu are nobler than the Al matrix, while $MgZn_2$ and Mg_2Si secondary particles are not nobler than the Al matrix [30]. Thus, these secondary phases dissolved either slower or faster than the Al matrix, leading to an inhomogeneous oxide film with increased roughness at the substrate/oxide interface [24,30,31]. In addition, flaws in the oxide film increased with the increase of anodizing voltage and current density. ZHANG et al [32] believed that increased current density could accelerate the oxidation reactions, contributing to dissolution and heating of the anodic film, thereby perturbing structural order and continuity of the film.

When anodization was done at current density of 3 A/dm^2 (voltage held fixed), the oxide film thickness increased, as shown in Figs. 2(e−h) and in Table 2, from that obtained with 2 A/dm^2. ZHOU et al [18] also reported that oxide film thickness grows as the current density increases from 0.5 to 50 mA/cm^2 (0.05−5 A/dm^2), and this is mainly caused by reduced field-assisted ejection of Al^{3+} ions from the film. The dissolution of aluminum is a combination of chemical dissolution and that assisted by electric field. As the current density increases, the growth rate of oxide film increases with less dissolution by the sulfuric acid electrolyte [13].

The micrographs of oxide films are shown in Figs. 2(i, j) at voltages of 20 and 25 V, obtained at anodizing electrolyte temperature of 5 °C and constant current density of 2 A/dm^2. The film obtained at 25 V is rather uniform and substrate/oxide interface has no flaws, which is an improvement from 15 °C anodizing temperature. This matches the results of NA et al [33]. They found that the oxide films from anodizing at 2 °C were more uniform than those obtained at 10 °C or 15 °C, for a constant anodizing time. The film thickness

from anodizing at 5 °C was 3.33 μm at 20 V and increased to 9.07 μm at 25 V, which are below those obtained at 15 °C with the same voltages. The effects of anodizing temperature are associated with the mass transfer rates of O^{2-} and Al^{3+} ions, and at the higher temperatures they form the Al_2O_3 film more rapidly [16]. Dense oxide films can be obtained at comparatively low temperatures with low sulfuric acid concentration [13].

On the other hand, the average hardness of oxide film decreased with the increase of film thickness and voltage, as shown in Table 2. Possibly, defects or flaws were formed in oxide films at higher anodizing voltages, thus reducing hardness. At the higher current density of 3 A/dm^2, the average hardness of oxide was lower than that from 2 A/dm^2 (voltage held fixed). However, the relation of hardness and voltage has the opposite trend when anodizing at 5 °C. The oxide film anodized with sulfuric acid electrolyte at 2 A/dm^2, 25 V, and 5 °C had the highest average hardness of HV 315. The loss of hardness with increasing electrolyte temperature was caused by increased porosity on the outer surface of the oxide layer [28].

The anodized specimens were dyed yellow before sealing. The color was quantified in color coordinates *L* and *b*, shown in Table 2. The maximal *L* of 100 represents a perfect reflecting diffuser while its smallest value of 0 indicates black with complete absorption. The coordinate *b* has no numeric bounds; it represents yellowness with positive values and blueness with negative values. The results showed that *L* decreased with voltage increasing from 15 to 25 V, and thereafter remained steady at 30 V. The trend in *b* is opposite to that of *L*. These color coordinates are related to surface morphology and internal structure of the anodized specimen, and these were markedly affected by the voltage in the sulfuric acid electrolyte, matching the results in Ref. [24].

3.3 Characteristics of oxide films on superheated slurry cast 7075 Al alloy substrate after anodizing in mixed electrolytes

Figure 4 shows cross-sections of oxide films on superheated slurry 7075 Al alloy substrates obtained with five mixed electrolytes: 55 mL/L H_2SO_4 + 30.92 g/L H_3BO_3, 55 mL/L H_2SO_4 + 61.83 g/L H_3BO_3, 109 mL/L H_2SO_4 +61.83 g/L H_3BO_3, 55 mL/L H_2SO_4 + 153.4 g/L $C_6H_8O_7$, and 109 mL/L H_2SO_4 + 315.21 g/L $C_6H_8O_7$, all at 2 A/dm^2, 15 °C, 25 V and 60 min. The substrate/oxide interface of H2-B2-2-25-15 sample (109 mL/L H_2SO_4 + 61.83 g/L H_3BO_3) in Fig. 4(c) is rather linear with some defects. In contrast, the interfaces of the other samples are clearly disturbed by the secondary phase particles, so that irregular and flawed interfaces can be seen in Figs. 4(a, b, d, e).

The thicknesses, hardness, and color of the anodic oxide film were measured and given in Table 2. The anodic oxide film thickness was affected by the type and concentration of the mixture electrolyte. SHIH and TZOU [14] also found that the oxide film thickness increased with the increase of the concentration of boric acid. In addition, oxide films anodized in these mixed electrolytes had higher thickness than that obtained with sulfuric acid at 2 A/dm^2, 25 V, 15 °C and 60 min. It was found that the oxide film anodized in the mixed electrolyte H_2SO_4 (109 mL/L) + $C_6H_8O_7$ (315.21 g/L) had the highest thickness of 24.81 μm and also the highest average hardness. Citric acid is stronger than boric acid, so citric acid can dissolve more Al^{3+} to react with the O^{2-} in the electrolyte, and it therefore forms thicker Al_2O_3 film [14]. The hardness of oxide film also

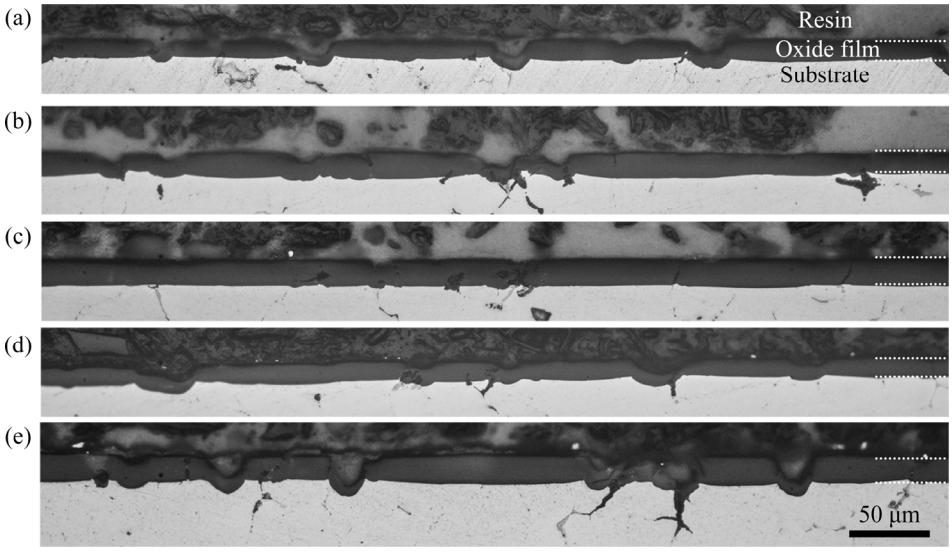

Fig. 4 Cross-section micrographs of anodized oxide films (white dashed lines show oxide film boundaries): (a) H1-B1-2-25-15; (b) H1-B2-2-25-15; (c) H2-B2-2-25-15; (d) H1-CH1-2-25-15; (e) H2-CH2-2-25-15

increased with the increase of the concentration of $C_6H_8O_7$, when mixed with $C_6H_8O_7$ and H_2SO_4. The highest hardness of oxide film was HV (347.04±40.34), obtained with 315.21 g citric acid mixed with sulfuric acid, while the mixture of boric acid and sulfuric acid as electrolyte gave lower hardness. This is caused by the intensity of chemical dissolution depending on citric acid concentration. Some citrate ions also migrated into the porous coating, increasing thickness of the oxide film [34]. However, the standard deviations of hardness measurements (Table 2) for samples anodized in these mixed electrolytes were greater than those with sulfuric acid electrolyte, indicating poorer uniformity of the coating [23].

On the other hand, the color coordinates *L* and *b* were similar to all sulfuric−boric acid mixed electrolytes, indicating similar surface morphologies. The coordinates obtained with mixed sulfuric−citric acid electrolytes were lower than those with sulfuric−boric acid electrolytes, indicating a difference in the surface morphologies.

3.4 Surface morphologies of oxide films on superheated slurry cast 7075 Al alloy substrates

Five anodized samples H1-2-15-15, H1-2-25-15, H1-2-25-5, H2-B2-2-25-15, and H2-CH2-2-25-15 were examined for surface morphology by FE-SEM, as shown in Fig. 5. The oxide films on these samples had different anodizing electrolytes, voltages, and temperatures. Holes are seen on the oxide films in Figs. 5(a_1), (b_1), (c_1), (d_1), and (e_1). Some secondary particles were dissolved during the anodizing and left holes on the surfaces [24]. The shallow holes in the oxide film of H2-CH2-2-25-15 case (Fig. 5(e_1)) are the largest in both size and number, while the surface of H1-2-25-15 case in Fig. 5(b_1) is very poor relative to the other four anodized samples. The oxide film on H1-2-25-5 is rather smooth with a few shallow holes (Fig. 5(c_1)). The high magnification FE-SEM images in Figs. 5(a_2), (b_2), (c_2), (d_2) and (e_2) show top views of the porous oxide films. Nano-pore diameter of the H1-2-15-15 case (Fig. 5(a_2)) is very small, and its areal fraction on the oxide film surface is 0.138. On increasing the anodizing voltage to 25 V (case H1-2-25-15), the nano-pores became larger in size and irregular with non-uniform shapes (Fig. 5(b_2)), and the areal fraction grew to 0.318. It could also be observed that at some locations the oxide walls between neighboring pores were completely dissolved so that the pore mouths merged, which increased the areal fraction of pores. This result conflicts with the prior study by BENSALAH et al [13]. They found that the porosity of oxide layer decreased with the increase of the voltage when anodizing in sulfuric acid electrolyte at 5.3 °C.

Moreover, the electrolyte temperature also affected the oxide dissolution and porous oxide structure [28]. When the anodizing temperature was decreased to 5 °C for the H1-2-25-5 sample, the size and shape of nano-pores were rather uniform compared to that at 15 °C, as seen in Fig. 5(c_2). In addition, the nano-pore areal fraction was found to be 0.043. Therefore, decreasing the electrolyte temperature reduced oxide dissolution and gave a less porous oxide structure near the surface. In the case of mixed electrolytes, the oxide films anodized in sulfuric−boric acid (H2-B2-2-25-15 sample) and sulfuric−citric acid (H2-CH2-2-25-15 sample) had small diameter pores compared to H1-2-25-15, with pore areal fractions being 0.167 and 0.049, respectively, as seen in Figs. 5(d_2) and (e_2), respectively. Besides, the areal fraction of nano-pores on the surface of oxide film is related to hardness, as shown in Fig. 6. It can be noted that the areal fractions of nano-pores are low, so these were comparatively dense oxide films with high hardness.

3.5 Corrosion resistance of oxide films on superheated slurry cast 7075 Al alloy substrate

The corrosion resistance of anodic oxide film was tested according to ASTM G31−72 (2004). The results are corrosion rates of the films in millimeter per year (mm/a), summarized in Table 3. The superheated slurry cast 7075 Al alloy substrate without anodization (Al 7075-T6) had the highest average corrosion rate of 0.065 mm/a. The oxide films reduced the corrosion rate, improving corrosion resistance. Anodization in sulfuric acid at 2 A/dm^2, 25 V and 5 °C gave the oxide film on H1-2-25-5 with the lowest corrosion rate of 0.003 mm/a, film thickness of (9.07±1.21) μm, smooth interface, few defects, and low surface porosity. This resisted corrosion better than H1-2-25-15, H2-B2-2-25-15, or H2-CH2-2-25-15 with higher thickness values of (14.59±0.98), (22.78±1.18), and (24.81±1.30) μm, and anodized in sulfuric acid, sulfuric−boric acid, and sulfuric−citric acid, respectively, at 2 A/dm^2, 25 V, and 15 °C. Although LI et al [35] reported that the corrosion rate of anodic film decreased with the increase of film thickness, this relationship did not hold in the current study generally, although it appeared true on comparing anodizing at 15 or 25 V with other conditions held constant (H_2SO_4 55 mL/L, 2 A/dm^2, and 15 °C). The film thickness increased from (2.78±0.83) to (14.59±0.98) μm on going from 15 to 25 V, and the corrosion rate decreased from 0.032 to 0.016 mm/a.

Figure 7 shows cross-sections of Al7075-T6 and the anodized Al7075-T6 samples after corrosion test. The Al7075-T6 sample was severely corroded in matrix α-Al with propagation of intergranular corrosion, as revealed in Fig. 7(a), and the intermetallic phase particles at grain boundaries were sensitive to chloride-induced

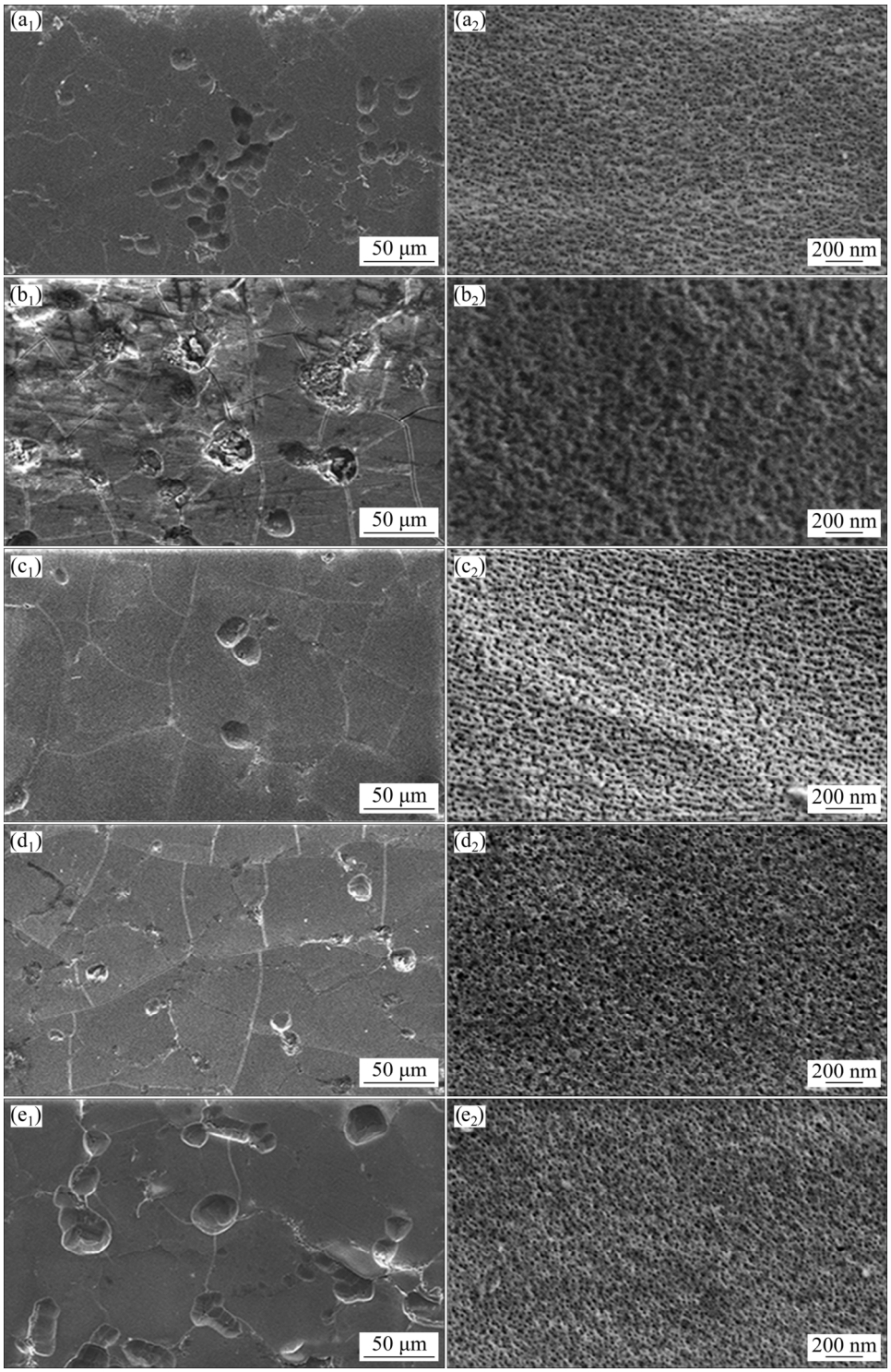

Fig. 5 FE-SEM images of anodized surfaces for H1-2-15-15 (a_1, a_2), H1-2-25-15 (b_1, b_2), H1-2-25-5 (c_1, c_2), H2-B2-2-25-15 (d_1, d_2), and H2-CH2-2-25-15 (e_1, e_2)

corrosion [30]. Moreover, corrosion pitting is evident in images of the anodized samples H1-2-15-15, H1-2-25-15, H2-B2-2-25-5, and H2-CH2-2-25-15, shown in Figs. 7(b, c, e, f). The case H1-2-15-15 (anodized in H_2SO_4 (55 mL/L), 2 A/dm^2, 15 V, and 15 °C) had very thin oxide film and few flaws, and had relatively poor corrosion resistance with severe uniform corrosion attack into matrix α-Al and propagation of localized corrosion in the anodized alloy, as shown in Fig. 7(b). The corrosion pits probably originated at cracks in the oxide film, matching the analysis of DEJUN and JINCHUN [36]. They proposed that corrosion pitting appeared at defects in the oxide film during early corrosion, and with further corrosion the pitting depth

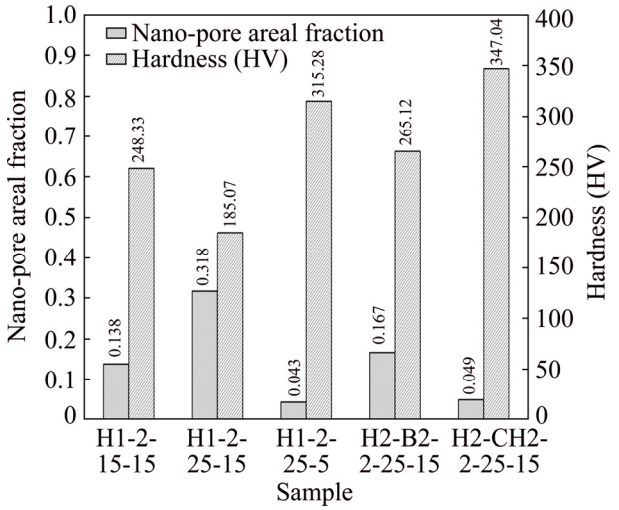

Fig. 6 Nano-pore areal fraction and hardness of oxide films

Table 3 Average corrosion rate of anodic oxide layer on as-cast 7075 Al alloy

Sample	Exposure duration/h	Average corrosion rate/(mm·a^{-1})
Al 7075-T6	168	0.065
H1-2-15-15	336	0.032
H1-2-25-15	336	0.016
H1-2-25-5	336	0.003
H2-B2-2-25-15	336	0.013
H2-CH2-2-25-15	336	0.008

expanded gradually, and various corrosion pits began to connect with each other. The Cl^- ions from NaCl in the salt spray test are the active anions with strong adsorption capacity and erosiveness, which mainly cause pitting [36,37]. Interestingly, the corrosion resistance of case H1-2-15-5 (anodized in H_2SO_4 (55 mL/L), 2 A/dm^2, 25 V, 5 °C) was superior to those of the other anodized samples. Corrosion pitting did not happen in the anodized sample, as seen in Fig. 7(d), because the oxide film was uniform and continuous. JOHN et al [34] reported that the oxide film on aluminum anodized in sulfuric/citric/boric acid electrolyte system exhibited better pitting corrosion resistance than that obtained in sulfuric electrolyte. In contrast, pitting corrosion resistance of a sample anodized in sulfuric acid in the present work was superior to those anodized in sulfuric−boric or sulfuric−citric acid mixtures. However, the anodization in sulfuric acid electrolyte should be done at the temperatures lower than 5 °C.

4 Conclusions

(1) The superheated slurry cast 7075 Al alloy substrate with secondary particles in the microstructure could be appropriately anodized in 55 mL/L sulfuric electrolyte at 2 A/dm^2, 25 V and 5 °C, so that the porous oxide film formed on the alloy was uniform with high hardness of about HV 315 and thickness of about 9 μm with excellent corrosion resistance.

(2) The thickness of oxide film increased with voltages from 15 to 30 V, and with current density from 2 to 3 A/dm^2, when anodizing in sulfuric acid electrolyte at 15 °C for 60 min.

(3) The alloy anodized in the mixed electrolytes of sulfuric−boric acid and sulfuric−citric acid had thicker oxide film than that anodized in sulfuric acid electrolyte.

(4) The hardness of oxide film was not tightly related to film thickness, but it varied with porosity of the film.

(5) Secondary particles in the microstructure of the alloy substrate formed defects in the oxide film and at oxide film/substrate interface, when the alloy was anodized in sulfuric acid or in sulfuric acid mixed with either boric acid or citric acid, at 2−3 A/dm^2, 15−30 V, and 15 °C.

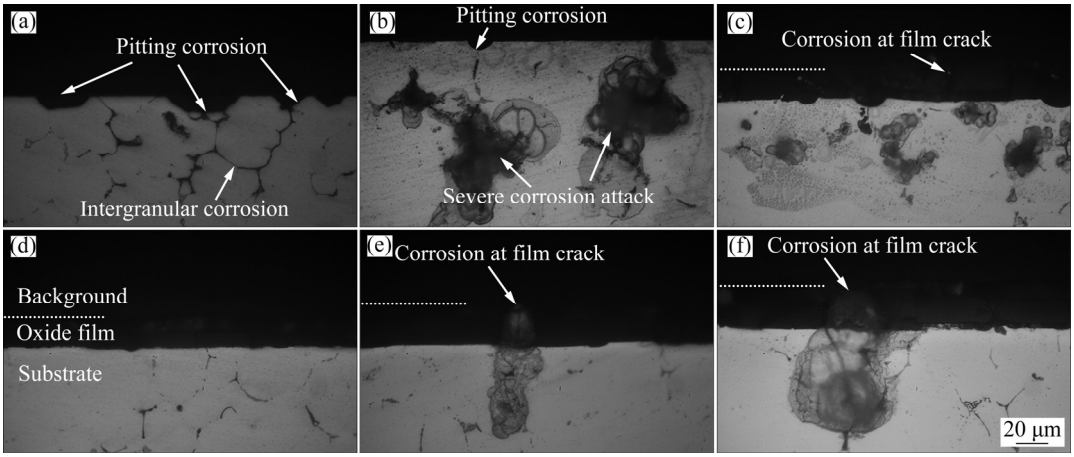

Fig. 7 Corrosion micrographs of specimens after immersion in NaCl (white dashed lines indicate surfaces of oxide film): (a) Al7075-T6; (b) H1-2-15-15; (c) H1-2-25-15; (d) H1-2-25-5; (e) H2-B2-2-25-15; (f) H2-CH2-2-25-15

Acknowledgments

This work was financially supported by the Higher Education Research Promotion and the National Research University Project of Thailand, Office of the Higher Education (Contract No. ENG580529S), Center of Excellence in Materials Engineering (CEME), the Graduate Engineer Scholarship and the Graduate School Scholarship, Prince of Songkla University, including Surat Thani Campus (2016). The authors also would like to thank the Department of Mining and Materials Engineering, Faculty of Engineering, Prince of Songkla University for laboratory facilities.

References

[1] WANNASIN J, JANUDOM S, RATTANOCHAIKUL T, CANYOOK R. Research and development of gas induced semi-solid process for industrial applications [J]. Transactions of Nonferrous Metals Society of China, 2010, 20(S3): s1010−s1015.

[2] LIU D, ATKINSON H V, KAPRANOS P, JIRATTITICHAROEAN W, JONES H. Microstructural evolution and tensile mechanical properties of thixoformed high performance aluminium alloys [J]. Materials Science and Engineering A, 2003, 361: 213−224.

[3] CURLE U A, GOVENDER G. Semi-solid rheocasting of grain refined aluminum alloy 7075 [J]. Transactions of Nonferrous Metals Society of China, 2010, 20(S3): s832−s836.

[4] DONG J, CUI J Z, LE Q C, LU G M. Liquidus semi-continuous casting, reheating and thixoforming of a wrought aluminum alloy 7075 [J]. Materials Science and Engineering A, 2003, 345: 234−242.

[5] CHUCHEEP T, WANNASIN J, CANYOOK R, RATTANOCHAIKUL T, JANUDOM S, WISUTMETHANGOON S, FLEMINGS M C. Characterization of flow behavior of semi-solid slurries with low solid fractions [J]. Metallurgical and Materials Transactions A, 2013, 44: 4754−4763.

[6] MAHATHANINWONG N, WISUTMETHANGOON S, PLOOPHOL T, WANNASIN J. Influence of solution heat treatment on microstructures of semisolid cast 7075 aluminium alloy [J]. Advance Materials Research, 2011, 33: 371−374.

[7] MAHATHANINWONG N, WISUTMETHANGOON S, PLOOKPHOL T, WANNASIN J. T6 heat treatment of rheocasting 7075 Al alloy [J]. Materials Science and Engineering A, 2012, 532: 91−99.

[8] MAHATHANINWONG N, WISUTMETHANGOON S, CHUCHEEP T, JANUDOM S, CANYOOK R. Precipitate coarsening parameters for gas induced semi-solid cast 7075-T6 Al alloy determined by SAXS measurements [J]. Bulletin of Materials Science, 2017, 40: 1513−1518.

[9] MAHATHANINWONG N, ZHOU Y, BABCOCK S E, PLOOKPHOL T, WANNASIN J, WISUTMETHANGOON S. Creep rupture behavior of semi-solid cast 7075-T6 Al alloy [J]. Materials Science and Engineering A, 2012, 556: 107−113.

[10] MAHATHANINWONG N, WISUTMETHANGOON S, PLOOKPHOL T, WANNASIN J, CHANTARAMANEE S. Elevated temperature tensile behavior of rheo-cast 7075-T6 al alloy produced by GISS technique [J]. Advance Materials Research, 2014, 881−883: 1597−1600.

[11] THANABUMRUNGKUL S, JANUDOM S, WANNASIN J. Industrial development of gas induced semi-solid process [J]. Transactions of Nonferrous Metals Society of China, 2010, 20(S3): s1016−s1021.

[12] IEWKITTAYAKORN I, JANUDOM S, MAHATHANINWONG N. Solution heat treatment of 7075 aluminum alloy affected on anodic oxide layer [J]. Materials Research Forum, 2016, 867: 19−23.

[13] BENSALAH W, FEKI M, WERY M, AYEDI H F. Thick and dense anodic oxide layers Formed on aluminum in sulphuric acid bath [J]. Journal of Materials Science and Technology, 2010, 26: 113−118.

[14] SHIH H H, TZOU S L. Study of anodic oxidation of aluminum in mixed acid using a pulsed current [J]. Surface and Coatings Technology, 2000, 124: 278−285.

[15] HAFEZI B. The effect of sulfuric acid on pore initiation in anodic alumina formed in oxalic acid [J]. Iranian Chemical Communication, 2014, 2: 222−231.

[16] MUBAROK M, UHO W, SUTARNO S, WAHYUDI S. Effects of anodizing parameters in tartaric−sulphuric acid on coating thickness and corrosion resistance of Al 2024 T3 alloy [J]. Journal of Minerals and Materials Characterization and Engineering, 2015, 3: 154−163.

[17] THEOHARI S, KONTOGEORGOU C. Effect of temperature on the anodizing process of aluminum alloy AA 5052 [J]. Applied Surface Science, 2013, 284: 611−618.

[18] ZHOU F, BARON-WIECHE A, GARCIA-VERGARAB S J, CURIONIA M, HABAZAKI H, SKELDON P, THOMPSONA G E. Effects of current density and electrolyte temperature on the volume expansion factor of anodic alumina formed in oxalic acid [J]. Electrochimica Acta, 2012, 59: 186−195.

[19] FRATILA-APACHITEIA L E, TERRYNB H, SKELDON P, THOMPSON G E, DUSZCZYKA J, KATGERMANA L. Influence of substrate microstructure on the growth of anodic oxide layers [J]. Electrochimica Acta, 2004, 49: 1127−1140.

[20] de SAENZ MIERA M, CURIONI M, SKELDON P, THOMPSON G E. The behaviour of second phase particles during anodizing of aluminium alloys [J]. Corrosion Science, 2010, 52: 2489−2497.

[21] MUKHOPADHYAY A K. On the nature of the Fe-bearing particles influencing hard anodizing behavior of AA 7075 extrusion products [J]. Metallurgical and Materials Transactions A, 1998, 29: 979−987.

[22] MUKHOPADHYAY A K, SHARMA A K. Influence of Fe-bearing particles and nature of electrolyte on the hard anodizing behaviour of AA 7075 extrusion products [J]. Surface and Coatings Technology, 1997, 92: 212−220.

[23] HAN Y D, JING H Y. Effect of Ni-coated carbon nanotubes on interfacial reaction and shear strength of Sn−Ag−Cu solder joints [J]. Journal of Electronic Materials, 2012, 41: 2478−2486.

[24] HAKIMIZAD A, RAEISSI K, ASHRAFIZADEH F. Characterization of aluminum anodized layers modified in sulfuric and phosphoric acid baths and their effect on conventional electrolytic coloring [J]. Surface and Coatings Technology, 2012, 206: 2438−2445.

[25] FRATILA-APACHITEI L E, DUSZCZYK J, KATGERMAN L. Vickers microhardness of AlSi (Cu) anodic oxide layers formed in H_2SO_4 at low temperature [J]. Surface and Coatings Technology, 2003, 165: 309−315.

[26] ASTM G 31–72. Standard practice for laboratory immersion testing of metals [S]. West Conshohocken, PA: ASTM International, 2014.

[27] AJEEl S A, ABDUL-HUSSEIN B A, KASSER N W. Breakdown and pitting formation of anodic film aluminum alloy (3003) [J]. Modern Applied Science, 2010, 4(5): 87−101.

[28] AERTS T. Influence of the anodizing temperature on the porosity and the mechanical properties of the porous anodic oxide film [J].

Surface and Coatings Technology, 2007, 201: 7310−7317.

[29] HUANG Y S, SHIH T S, CHOU J H. Electrochemical behavior of anodized AA7075-T73 alloys as affected by the matrix structure [J]. Applied Surface Science, 2013, 283: 249−257.

[30] BIRBILIS N, BUCHHEIT R G. Electrochemical characteristics of intermetallic phases in aluminum alloys an experimental survey and discussion [J]. Journal of the Electrochemical Society, 2005, 152: B140−B151.

[31] ZHOU X, THOMPSON G E, SKELDON P, WOOD G C, SHIMIZU K, HABAZAKI H. Film formation and detachment during anodizing of Al−Mg alloys [J]. Corrosion Science, 1999, 41: 1599−1613.

[32] ZHANG P, ZUO Y, ZHAO X, TANG Y, ZHANG X. Correlation between microhardness and microstructure of anodic film on 2024 aluminum alloy [J]. Journal of Wuhan University of Technology: Materials Science Edition, 2015, 30(3): 586−590.

[33] NA H C, SUNG T J, YOON S H, HYUN S K, KIM M S, LEE Y G, SHIN S H, CHOI S M, SUNG Y S. Formation of unidirectional nanoporous structures in thickly anodized aluminum oxide layer [J]. Transactions of Nonferrous Metals Society of China, 2009, 19: 1013−1017.

[34] JOHN P, KHAN I U, SHEIKH S T, GULZAR N, REHMAN A U. Improving pitting corrosion resistance of aluminum by anodizing process [J]. Journal of the Chemical Society of Pakistan, 2013, 35(1): 72−76.

[35] LI Y D, ZHANG Y, LI S M, ZHAO P Z. Influence of adipic acid on anodic film formation and corrosion resistance of 2024 aluminum alloy [J]. Transactions of Nonferrous Metals Society of China, 2016, 26: 492−500.

[36] DEJUN K, JINCHUN W. Salt spray corrosion and electrochemical corrosion properties of anodic oxide film on 7475 aluminum alloy [J]. Journal of Alloys and Compounds, 2015, 632: 286−290.

[37] RODRIGUEZ J J, HERNANDEZ F J, GONZALEZ J E. The effect of environmental and meteorological variables on atmospheric corrosion of carbon steel, copper, zinc and aluminium in a limited geographic zone with different types of environment [J]. Corrosion Science, 2003, 45(4): 799−815.

过热浆铸 7075 铝合金的阳极氧化工艺参数

Itsaree IEWKITTHAYAKORN[1], Somjai JANUDOM[1,2],
Narissara MAHATHANINWONG[2,3], Seppo KARRILA[3], Jessada WANNASIN [1,2]

1. Department of Mining and Materials Engineering,
Faculty of Engineering, Prince of Songkla University, Hat Yai, Songkhla 90112, Thailand;
2. Center of Excellence in Materials Engineering (CEME),
Faculty of Engineering, Prince of Songkla University, Hat Yai, Songkhla 90112, Thailand;
3. Faculty of Science and Industrial Technology,
Prince of Songkla University, Surat Thani Campus, Surat Thani 84000, Thailand

摘　要：通过对过热浆铸 7075 铝合金基体阳极氧化工艺参数包括电压、电流密度、温度和电解液的选择，确定合适的阳极氧化工艺参数。该合金阳极氧化所用溶液为硫酸电解液、硫酸与硼酸或柠檬酸的混合液。阳极氧化所用电压为 15~30 V，测试电流密度为 2 和 3 A/dm^2，温度为 5 和 15 °C。测试氧化膜的厚度、表面形貌、硬度和耐腐蚀性。结果发现，该合金在硫酸溶液中阳极氧化的最佳参数为 25 V、2 A/dm^2 和 5 °C。此条件下形成的氧化膜表面光滑且厚度均一、孔隙率低、硬度高，且具有最优的耐腐蚀性。然而，在较高温度(15 °C)下进行阳极氧化时，可以观察到不连续的氧化膜。所用替代电解质是硫酸与硼酸或柠檬酸的混合溶液。结果表明，硼酸和柠檬酸电解液均能提高氧化膜的厚度、硬度、耐蚀性和品质。 但是，这些氧化膜的性能仍然比不上合金在硫酸电解液中低温下(25 V, 2 A/dm^2，5 °C)形成的氧化膜的性能。

关键词：7075 铝合金；过热浆料铸造；阳极处理；氧化膜；阳极氧化参数

(Edited by Wei-ping CHEN)